Structural and thermodynamic study of Cs$_3$Na(MoO$_4$)$_2$
Margin to the safe operation of sodium cooled fast reactors

Smith, A. L.; Kauric, G.; van Eijck, L.; Goubitz, K.; Clavier, N.; Wallez, G.; Konings, R. J.M.

Citation (APA)
Smith, A. L., Kauric, G., van Eijck, L., Goubitz, K., Clavier, N., Wallez, G., & Konings, R. J. M. (2019). Structural and thermodynamic study of Cs$_3$Na(MoO$_4$)$_2$: Margin to the safe operation of sodium cooled fast reactors. *Journal of Solid State Chemistry*, *269*, 1-8. https://doi.org/10.1016/j.jssc.2018.08.033

Important note
To cite this publication, please use the final published version (if applicable).
Please check the document version above.

Structural and thermodynamic study of $Cs_3Na(MoO_4)_2$: Margin to the safe operation of Sodium cooled Fast Reactors

A.L. Smith[a,*], G. Kauric[b], L. van Eijck[a], K. Goubitz[a], N. Clavier[c], G. Wallez[d], R.J.M. Konings[e]

[a] Delft University of Technology, Faculty of Applied Sciences, Radiation Science & Technology Department, Mekelweg 15, 2629 JB Delft, The Netherlands
[b] PSL Research University, Chimie ParisTech-CNRS, Institut de Recherche de Chimie Paris, 75005 Paris, France
[c] Institut de Chimie Séparative de Marcoule, UMR 5257 CEA/CNRS/ENSCM/Univ. Montpellier, Site de Marcoule-Bât. 426, 30207 Bagnol/Cèze, France
[d] Sorbonne University, UPMC Université Paris 06, 75005 Paris, France
[e] European Commission, Joint Research Centre-Karlsruhe (JRC), P.O. Box 2340, D-76125 Karlsruhe, Germany

Abstract

Neutron diffraction measurements of the double molybdate $Cs_3Na(MoO_4)_2$ have been performed for the first time in this work and the crystal structure refined using the Rietveld method. The thermal expansion of this trigonal phase, in space group $P\bar{3}m1$, measured using high temperature X-ray diffraction (XRD), remains moderate: $\alpha_a = 31{\cdot}10^{-6}$ K^{-1} and $\alpha_c = 24{\cdot}10^{-6}$ K^{-1} in the temperature range T=(298-723) K. The melting temperature of this compound has been determined at $T_{fus} = (777 \pm 5)$ K using Differential Scanning Calorimetry (DSC). No phase transition was detected, neither by DSC, nor by high temperature XRD or high temperature Raman spectroscopy, which disagrees with the literature data of Zolotova et al. (2016), who reported a reversible phase transition around 663 K. Finally, thermodynamic equilibrium calculations have been performed to assess the probability of formation of $Cs_3Na(MoO_4)_2$ inside the fuel pin of a Sodium cooled Fast Reactor by reaction between the cesium molybdate phase Cs_2MoO_4, which forms at the pellet rim at high burnup, the fission product molybdenum (either as metallic or oxide phase), and the liquid sodium coolant in the accidental event of a breach of the stainless steel cladding and sodium ingress in the failed pin.

Keywords: Neutron diffraction, X-ray diffraction, Raman spectroscopy, Differential Scanning Calorimetry, Double molybdates

*Corresponding author
  Email address: `a.l.smith@tudelft.nl` (A.L. Smith)

1. Introduction

Double molybdates of the form $A_nR_m(MoO_4)_2$ (A= alkalis, alkaline-earths, Cu, Tl; R= rare earth elements, Bi, Pb, Zn) have been studied extensively in the past few years because of their exciting properties as phosphors luminescent materials [1, 2], solid state lasers [3, 4], ferroelastics and ferroelectrics [5–7]. Phases such as $A_3LiZn_2(MoO_4)_4$ (A=Rb, Cs) and $Cs_3LiCo_2(MoO_4)_4$ have also been reported [8, 9], with promising properties as solid-lithium ion conductors [10]. While studying the phase formations in the Na_2MoO_4-Cs_2MoO_4-Zn_2MoO_4 system, and the possible insertion of sodium into the $Cs_6Zn_5(MoO_4)_8$ structure, Zolotova et al. [10] recently reported two new phases, namely $Cs_3Na(MoO_4)_2$ and $Cs_3NaZn_2(MoO_4)_4$. The authors re-investigated the poorly known Na_2MoO_4-Cs_2MoO_4 system, which is of particular interest for the safety assessment of next generation Sodium cooled Fast Reactors (SFRs).

During irradiation of the mixed oxide $(U_{1-y}Pu_y)O_{2-x}$ fuel (MOX) in fast neutrons reactors such as SFRs, the fission products cesium, molybdenum, iodine and tellurium are generated with a high fission yield [11]. Because of the high volatility of the latter products and the strong axial temperature gradient ($\sim$ 450 K·mm^{-1} with $\sim$ 2273 K in the centre and $\sim$ 973 K at the pellet rim) in the fuel pin, they migrate after formation towards the pellet rim, where they accumulate in the space between fuel and cladding. Post-irradiation examinations of fuel pins irradiated in the Phénix reactor [11] have demonstrated the formation of a multi-component phase, the so-called JOG phase (Joint Oxide Gain), whose main constituents are Cs_2MoO_4, CsI, Cs_2Te, and Cs_2UO_4 [12, 13].

One of the important safety considerations for the operation of SFRs concerns the risk of a breach of the stainless steel cladding during normal operation or accidental conditions. Although extremely rare, such clad breach can occur due to manufacturing defaults in the cladding material, fuel cladding mechanical or chemical interaction [14], due to blocking of a coolant channel or unexpected change in the neutron flux [15]. A thorough safety assessment of the reactor therefore requires to consider the aftermath of an accidental ingress of sodium in a failed pin. Past studies have suggested that sodium could substitute cesium in the main component of the JOG phase, namely cesium molybdate, leading to sodium molybdate formation in the gap between fuel and cladding, and reduction of the cesium to cesium metal: $2Na + Cs_2MoO_4 = 2Cs + Na_2MoO_4$ [16]. This assumption is still subject of controversy, however, and the studies of Tête in 1999 using thermal analysis and scanning electron microscopy suggested no cesium-sodium substitution, but rather the formation of cesium, sodium and molybdenum oxides [15]. The phase relationships in the Cs_2MoO_4-Na_2MoO_4 system have been investigated by X-ray diffraction and thermal analysis as early as 1964 [17], but it is only very recently that the formation of the quaternary phase $Cs_3Na(MoO_4)_2$ has been established. Given the remaining uncertainties regarding the product of the sodium-cesium molybdate interaction, a comprehensive structural and thermodynamic characterization of the $Cs_3Na(MoO_4)_2$ phase is necessary.

In this work, we report for the first time neutron diffraction measurements

at room temperature of $Cs_3Na(MoO_4)_2$, the study of its thermal expansion behaviour and polymorphism using high-temperature X-ray diffraction, Differential Scanning Calorimetry, and high-temperature Raman spectroscopy. Using the thermodynamic functions newly measured in our research group for this compound [18], the probability of the formation of $Cs_3Na(MoO_4)_2$ in the fuel pin by reaction of the sodium coolant with Cs_2MoO_4 was finally assessed.

2. Experimental methods

2.1. Sample preparation

$Cs_3Na(MoO_4)_2$ was synthesized by reaction between accurately weighted quantities of cesium molybdate Cs_2MoO_4 and sodium molybdate (Na_2MoO_4 anhydrous, 99.9% trace metal basis, Sigma-Aldrich). The cesium molybdate starting material was synthesized as described in [19]. The stoichiometric mixture was heated under argon inside a tightly closed stainless steel container at 723 K for 200 h, with intermediate regrinding steps. Because of the molybdates' hygroscopic nature, handling was done exclusively inside the dry atmosphere of an argon-filled glove box. The purity of the sample was examined by X-ray and neutron diffraction at room temperature, Differential Scanning Calorimetry (DSC), and ICP-MS analysis. No secondary phases were detected by XRD and neutron diffraction. The DSC measurements showed a single peak in the heat flow signal as a function of temperature, corresponding to the melting event, as detailed in section 3.2. No additional peaks could be assigned to impurities. The ICP-MS analysis yielded a cesium-to-molybdenum ratio of (1.44 ± 0.07[1]) at/at and a sodium to molybdenum ratio of (0.51 ± 0.03[2]), which corresponds to the global composition $Cs_{2.88(\pm0.14)}Na_{1.02(\pm0.06)}(MoO_4)_2$, hence within uncertainties, in good agreement with the stoichiometric formula. The sample purity is expected to be better than 99 wt%.

2.2. Neutron diffraction

Neutron diffraction data were recorded on the beamline PEARL at the Hoger Onderwijs Reactor at TU Delft [20]. The sample was encapsulated in a vanadium cylindrical container (50 mm high, 6 mm inner diameter) closed with a viton o-ring. The data were collected at room temperature, at a fixed wavelength ($\lambda = 1.667$ Å) for 30 h over the range $11° \leq 2\theta \leq 158°$. Structural analysis was performed by the Rietveld method with the Fullprof2k suite [21].

---

[1] The uncertainty is an expanded uncertainty $U=k·u_c$ where u_c is the combined standard uncertainty estimated following the ISO/BIPM Guide to the Expression of Uncertainty in Measurement. The coverage factor is $k=2$.

[2] The uncertainty is an expanded uncertainty $U=k·u_c$ where u_c is the combined standard uncertainty estimated following the ISO/BIPM Guide to the Expression of Uncertainty in Measurement. The coverage factor is $k=2$.

2.3. Powder X-ray diffraction

The X-ray diffraction measurements were carried out at room temperature using a PANalytical X'Pert PRO X-ray diffractometer mounted in the Bragg-Brentano configuration with a Cu anode (0.4 mm x 12 mm line focus, 45 kV, 40 mA). The X-ray scattered intensities were measured with a real time multi strip (RTMS) detector (X'Celerator). The data were collected by step scanning in the angle range $10° \leq 2\theta \leq 120°$ with a step size of $0.008°$ (2θ); total measuring time was about 8 h.

2.4. High temperature X-ray diffraction

The thermal expansion and polymorphism of $Cs_3Na(MoO_4)_2$ were also investigated by high temperature X-ray diffraction using the same diffractometer equipped with an Anton Paar TTK450 chamber. Measurements were conducted under vacuum (0.02 mbar) from room temperature up to 723 K, with 50 K heating steps. The temperature was measured with a Pt100 resistor. Each temperature plateau was maintained for 6 h after a stabilisation time of 30 min.

2.5. Differential Scanning Calorimetry

3D-heat flow DSC measurements were moreover performed up to 853 K using a Setaram Multi HTC module of the 96 Line calorimeter. The sample (96.7 mg) was placed in a nickel liner and encapsulated for the calorimetric measurements in a stainless steel crucible closed with a screwed bolt as described in [22] to avoid vaporization at high temperatures. The measurement program consisted in four successive heating cycles with 5 K·min^{-1} heating rate, and 2-5-10-15 K·min^{-1} cooling rates. The sensitivity of the corresponding measurement was around 0.443 μV·mW^{-1}. The temperatures were monitored throughout the experiments by a series of interconnected S-types thermocouples. The temperature on the heating ramp was calibrated by measuring the melting points of standard materials (Au, Ag, In, Al, Pb, Sn, Zn). The temperature on the cooling ramp was obtained by extrapolation to 0 K·min^{-1} cooling rate. The transition temperatures were derived on the heating ramp as the onset temperature using tangential analysis of the recorded heat flow.

2.6. High temperature Raman spectroscopy

High temperature Raman spectra were recorded using a Horiba Jobin-Yvon Aramis spectrometer equipped with a Linkam TS-1500 heating device. The $Cs_3Na(MoO_4)_2$ sample was placed in a platinum crucible and inserted in the furnace. A rate of 10 K/min was applied upon heating and 5 min of stabilisation time were maintained at each temperature plateau before acquisition of the spectrum. The 532 nm line of a Nd-YAG laser was used as excitation wavelength and focused by means of an Olympus BX41, thus delivering about 40 mW at the sample surface. Slits and confocal hole were set to result in a 1 cm^{-1} resolution. For each spectrum, an acquisition time of 3 s was considered with an average of 4 scans. Before analysis, the apparatus was calibrated with a silicon wafer, using the first-order Si line at 520.7 cm^{-1}. Band component analysis of the different

spectra was performed with the Jandel Peakfit software, using pseudo-Voigt functions with the minimum number of components. Correlation coefficients greater than 0.997 were systematically obtained.

3. Results and discussion

3.1. Structural refinement of $Cs_3Na(MoO_4)_2$ from neutron diffraction data

$Cs_3Na(MoO_4)_2$ shows a trigonal structure at room temperature, in space group $P\bar{3}m1$, belonging to the glaserite type, as shown by the recent single crystal studies of Zolotova et al. [10]. The X-ray and neutron diffraction patterns for this compound are shown in Figures 1 and 2. The refined cell parameters by XRD, a=6.34381(2) Å and c=8.21888(3) Å (note that the statistically derived s.u.'s are underestimated by about one order of magnitude), and neutron diffraction, a=6.3352(3) Å and c=8.2068(5) Å (note that the statistically derived s.u.'s are underestimated by about one order of magnitude), are in good agreement with those of [10]. The atomic positions derived from the Rietveld refinement of the neutron data are listed in Table 1 and selected bond lengths in Table 2.

$Cs_3Na(MoO_4)_2$ is made of layers of corner-sharing and alternating MoO_4 tetrahedra and NaO_6 octahedra in the (ab) plane. The MoO_4 tetrahedra are only slightly distorted with one Mo-O1 distance at 1.719(6) Å and three distances at 1.7650(14) Å, while the NaO_6 octahedra are regular with Na-O2 distances at 2.5416(12) Å. The cesium atoms, 12-fold (Cs1) and 10-fold (Cs2) coordinated, respectively, are found in between these layers and link them together.

Table 1: Refined atomic positions in $Cs_3Na(MoO_4)_2$ derived from the neutron refinement. R_{wp} = 9.95, R_{exp} = 4.18, χ^2 = 5.68. Background: Linear interpolation between operator-selected points in the pattern with refinable heights.

Atom	Ox. State	Wyckoff	x	y	z	$B_0(\text{Å}^2)$
Na	+1	1a	0	0	0	1.8(2)
Cs1	+1	1b	0	0	1/2	1.4(1)
Cs2	+1	2d	1/3	2/3	0.8292(5)	1.98(7)
Mo	+6	2d	1/3	2/3	0.2634(4)	1.67(6)
O1	-2	2d	1/3	2/3	0.4728(6)	4.38(9)
O2	-2	6i	0.1815(2)	0.8185(2)	0.1924(2)	1.91(3)

Table 2: Selected bond lengths in $Cs_3Na(MoO_4)_2$ derived from the neutron refinement.

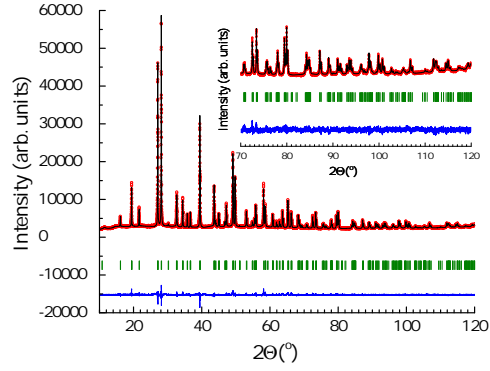| Bond	Bond length (Å)	Bond	Bond length (Å)
Cs1-O1 (x6)	3.6644(4)	Na-O2 (x6)	2.5416(12)
Cs1-O2 (x6)	3.2155(15)	Mo-O1 (x1)	1.719(6)
Cs2-O1 (x1)	2.924(7)	Mo-O2 (x3)	1.7650(14)
Cs2-O2 (x6)	3.1768(8)		
Cs2-O2 (x3)	3.415(4)		

Figure 1: Comparison between the observed (Y_{obs}, in red) and calculated (Y_{calc}, in black) X-ray diffraction patterns of $Cs_3Na(MoO_4)_2$. $Y_{obs} - Y_{calc}$, in blue, is the difference between the experimental and calculated intensities. The Bragg reflections' angular positions are marked in green. Measurement at λ=Cu-Kα.
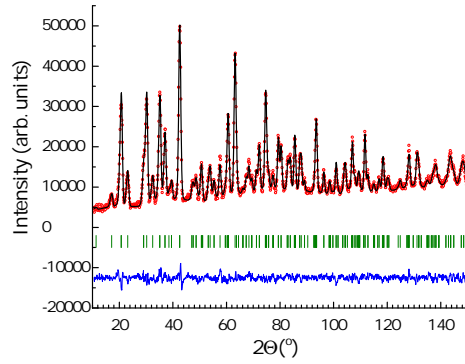

Figure 2: Comparison between the observed (Y_{obs}, in red) and calculated (Y_{calc}, in black) neutron diffraction patterns of $Cs_3Na(MoO_4)_2$. $Y_{obs} - Y_{calc}$, in blue, is the difference between the experimental and calculated intensities. The Bragg reflections' angular positions are marked in green. Measurement at λ=1.667 Å.
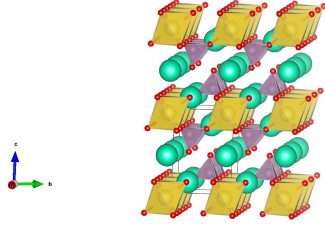
6

Figure 3: Crystal structure of $Cs_3Na(MoO_4)_2$: NaO_6 octahedra in yellow, MoO_4 tetrahedra in purple, Cs atoms in green, O atoms in red.

3.2. High temperature behaviour

In the event case $Cs_3Na(MoO_4)_2$ would form inside the fuel pin by reaction between the JOG phase and the sodium coolant, one needs to assess this compound's thermal expansion so as to predict the effect on the progress of the clad breach. The evolution of the lattice parameters with temperature was determined by Rietveld refinement of the high temperature X-ray diffraction data (see Table A.1). No change in the X-ray diffraction pattern was observed up to the maximum temperature of the measurement $T = 723$ K, except for a shift to lower 2θ values following the expansion of the unit cell. The relative thermal expansions of the a and c unit cell parameters are shown in Figure 4 between room temperature and T=723 K. The mean relative linear thermal expansion coefficient dl/l_0, where $l=(abc)^{1/3}$, can be expressed as a polynomial function of the temperature $T(K)$:

$$dl/l_0 = -5.64 \cdot 10^{-3} + 1.53667 \cdot 10^{-5}T + 1.28537 \cdot 10^{-8}T^2 \qquad (1)$$

where $l_0=(a_0 b_0 c_0)^{1/3}$ is the reference length at room temperature. The thermal expansion is rather high along the a ($\alpha_a \sim 31 \cdot 10^{-6}$ K^{-1}) and c ($\alpha_c \sim 24 \cdot 10^{-6}$ K^{-1}) axes, but the relative thermal expansion is about 35% lower at T=723 K than that of the cesium molybdate Cs_2MoO_4 (shown as dotted line in Figure 4).

Surprisingly, no change in the X-ray diffraction pattern was observed around $T = 663$ K, although Zolotova et al. [10] reported the existence of a reversible polymorphic transition at this temperature according to their DTA data. Differential Scanning Calorimetry measurements were performed to solve this discrepancy (Figure 5), but there again no sign of a phase transition could be detected around $T = 663$ K in the successive heating and cooling cycles. Only the melting transition was observed at $T_{fus} = (777 \pm 5)$ K, in good agreement with the DTA result of Zolotova et al. (783 K) [10]. The existence of a phase transition in this compound is hence not supported by the present XRD and DSC data. One could imagine, given the low temperature of the reported phase transition, that the synthesized phase corresponds to the high temperature β polymorph, quenched at room temperature during cooling. To rule out this hypothesis, an annealing treatment was performed for 80 h at 623 K, but this did not lead to
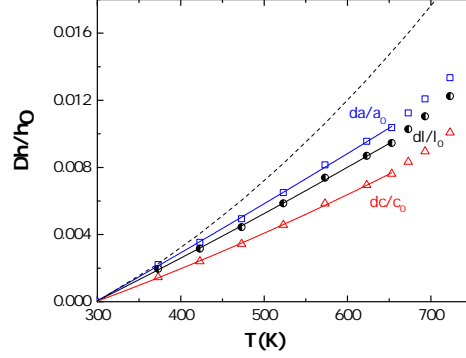
7

Figure 4: Linear thermal expansion of $Cs_3Na(MoO_4)_2$ along the crystallographic axes. The results of Wallez et al. [19] for the mean relative linear expansion dl/l_0 of orthorhombic Cs_2MoO_4 are shown with a dotted line for comparison.

any change in the X-ray diffraction pattern. In fact, Zolotova et al. also reported that "additional annealing of $Cs_3Na(MoO_4)_2$ at 350°C (623 K) gave no rise to a noticeable changing of the diffraction pattern, which may be explained by a negligible deformation of the structure below the polymorphic transition at 390°C" (663 K). The authors hence only observed the aforementioned transition by DTA. Since they do not show their measured DTA curves, we cannot judge if the corresponding feature simply corresponded to an artefact.
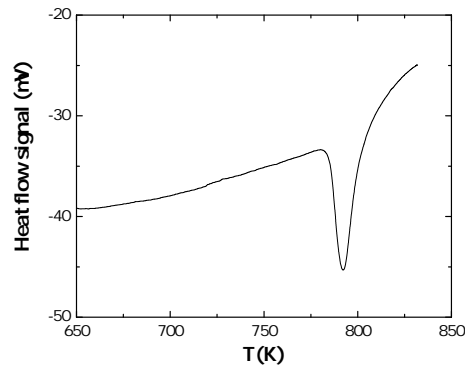

Figure 5: DSC output of the measurement of the $Cs_3Na(MoO_4)_2$ sample from room temperature up to $T=832$ K.

8

3.3. High temperature Raman spectroscopy

Five sets of bands resulting from the internal modes of vibration of the MoO_4 units can be distinguished in the Raman spectrum of $Cs_3Na(MoO_4)_2$ at room temperature, in good agreement with the data reported in the literature for $MeMoO_4$ (Me=Ca, Sr, Ba, Pb), and M_2MoO_4 (M=Cs, Na, Ag) molybdates [19, 23, 24]. The external (translational) modes ν_{ext} observed below 100 cm^{-1} results from the motion of the Cs^+ cations with respect to the rigid MoO_4 tetrahedra [25]. The vibrations found between 300 and 350 cm^{-1} correspond to the symmetric (ν_2) and antisymmetric (ν_4) bending modes, while those found between 780 and 900 cm^{-1} are attributed to symmetric (ν_1) and antisymmetric (ν_3) stretching modes [26].

No significant change of the Raman spectrum was observed up to $T = 773$ K, where the fusion of the sample occurred, in agreement with our X-ray diffraction data, and again in disagreement with the results of Zolotova et al. [10] concerning the existence of a phase transition around $T = 663$ K. Some shifts in the wavenumber and some slight changes in bandwidth were observed (see Appendix B), but these can be attributed to anharmonic effects with the temperature increase [25].
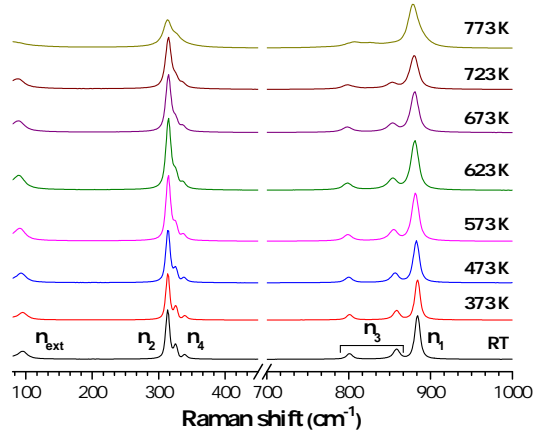

Figure 6: Variation of the Raman spectrum of $Cs_3Na(MoO_4)_2$ versus temperature.

3.4. Margin to the safe operation of Sodium cooled Fast Reactors

As mentioned in the introduction, the potential formation of $Cs_3Na(MoO_4)_2$ following a breach of the stainless steel cladding and ingress of sodium coolant inside the pin of a Sodium cooled Fast Reactor should be assessed since cesium and molydenum are produced with a high fission yield during irradiation [11]. Three different scenarios could be envisaged for this compound's formation,

9

and thermodynamic equilibrium calculations have been performed as detailed hereafter to assess their likelihood.

The condition for the reaction between the cesium molybdate (JOG phase), molybdenum, and sodium to occur depends on the amount of oxygen dissolved in the liquid sodium coolant and the oxidation state of molybdenum, which can form either as metallic precipitate or oxide phase depending on the burn-up, temperature and oxygen potential of the fuel.

Metallic precipitates formed of the five elements (Mo,Ru,Tc,Rh,Pd) have been observed in post-irradiation examinations (by EPMA) of MOX fuel as white inclusions, these precipitates becoming larger and larger with increasing burn-up and temperature [14]. Whereas all the (Ru,Tc,Rh,Pd) created by irradiation remain in the metallic form, the situation is more complex for molybdenum. At low burn-up, when the $U_{1-y}Pu_yO_{2-x}$ fuel is still hypostoichiometric (oxygen-to-metal O/M ratio~1.93-1.98 at the beginning of the irradiation), molybdenum is essentially in the metallic state [14]. However, each fission reaction releases two oxygen atoms, which are only partly consumed by the fission products. As a result, the oxygen-to-metal ratio of the fuel increases with burn-up together with the increase in the valence of Pu until it reaches the +IV oxidation state (U remains in all cases at the valence +IV), and the mixed oxide fuel becomes stoichiometric, i.e., $U_{1-y}Pu_yO_{2.0}$. When the stoichiometric composition is reached, which corresponds to a burnup threshold of 5-10 at.% (depending on the initial O/M fuel ratio), the oxygen potential of the fuel is such that molybdenum begins to oxidize into MoO_2 or Cs_2MoO_4 [14]. At high burn-up, molybdenum is finally mostly in the oxidized state, i.e. MoO_2, MoO_3 or Cs_2MoO_4, and acts as a buffer for the fuel whose oxygen-to-metal ratio is maintained close to 2.0 [14].

3.4.1. Formation from the reaction between cesium molybdate and molybdenum metal

In the scenario of an intermediate burn-up, one could imagine that metallic molybdenum, co-existing with Cs_2MoO_4, could react with the liquid sodium to form the $Cs_3Na(MoO_4)_2$ phase corresponding to the equilibrium reaction:

$$Na(l, O\text{in sln}) + 3/2Cs_2MoO_4(cr) + 1/2Mo(cr) + O_2(\text{dissolved in Na}) \rightleftharpoons Cs_3Na(MoO_4)_2(l) \tag{2}$$
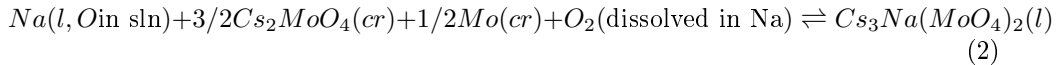
Considering the sodium quasi-pure, with very little oxygen dissolved, the partial Gibbs energy of sodium $\Delta \overline{G}_{Na}$ is taken to be zero, and the equilibrium oxygen potential for this reaction is given by:

$$\Delta \overline{G_{O_2}^{eq}}(T) = RTln(P_{O_2}/P^o) \tag{3}$$
$$= \Delta_f G_m^o(Cs_3Na(MoO_4)_2, l, T) - 3/2\Delta_f G_m^o(Cs_2MoO_4, cr, T) \tag{4}$$

where P_{O_2} is the pressure of oxygen, P^o the standard partial pressure equal to 1 bar, $\Delta_f G_m^o(Ca_3Na(MoO_4)_2, l, T)$ and $\Delta_f G_m^o(Cs_2MoO_4, cr, T)$ the Gibbs energies of formation of $Cs_3Na(MoO_4)_2$ and Cs_2MoO_4, respectively, R the universal gas constant, and T the temperature.

The temperature of the sodium coolant entering the reactor core is about 673 K, while the average temperature of sodium above the core is around 823 K [14]. The temperature of the fuel rim is expected to be slightly higher, in the range 893-923 K, while it may exceed 2273 K in the centre [14]. Supposing $Cs_3Na(MoO_4)_2$ would form, it would be in the liquid state at the temperatures of the fuel rim.

Using the thermodynamic functions listed in Table C.1 and C.2 for Cs_2MoO_4, and the enthalpy of formation and standard entropy of $Cs_3Na(MoO_4)_2$ recently determined in our research group [18], the oxygen potential threshold of formation of $Cs_3Na(MoO_4)_2$ was derived as $\Delta \overline{G_{O_2}^{eq}}(T/K) = -730120 + 183.60\,T$ J·mol^{-1} in the temperature range T=(371-777) K, and $\Delta \overline{G_{O_2}^{eq}}(T/K) = -669708 + 105.46\,T$ J·mol^{-1} for temperatures above $T = 777$ K. Note that the enthalpy of fusion of $Cs_3Na(MoO_4)_2$ is unknown, and was estimated for the purpose of this calculation using the procedure described in Appendix D. The high temperature heat capacity of $Cs_3Na(MoO_4)_2$ was also never measured experimentally, and estimated in this work using the Neumann-Kopp rule applied to the Cs_2MoO_4 and Na_2MoO_4 ternary constituting oxides (see Appendix C).

The threshold for the onset of the reaction between cesium molybdate, molybdenum and sodium should be compared to the concentration levels of oyxgen dissolved in liquid sodium. Combining the oxygen solubility equation in sodium reported in the critical review of Noden [27, 28] with the Gibbs energy of formation of sodium oxide Na_2O [29], the oxygen potential limit in sodium is given by $\Delta \overline{G_{O_2}^{eq}}(T/K) = -735691.3 + (33.232 + 38.287logC_O)T$ J·mol^{-1}, as described in detail in the work of [30], where C_0 is the concentration of oxygen dissolved in liquid sodium.

Figure 7 shows the oxygen potential threshold of formation of $Cs_3Na(MoO_4)_2$ compared to the oxygen potential lines for levels in sodium ranging from 0.1 wppm to 1000 wppm. It should be pointed out that in normal operating conditions oxygen levels are kept below circa 3 wppm [31] in SFRs to avoid corrosion issues of the containment material [32]. Looking at figure 7, one can see that an oxygen concentration of almost 10^4 wppm is necessary at T=900 K to form $Cs_3Na(MoO_4)_2$ from Cs_2MoO_4 and Mo metal, hence much higher levels than in the typical operating range of SFRs. The latter reaction, is hence to be completely excluded.

3.4.2. Formation from the reaction between cesium molybdate and molybdenum oxide

In a similar manner to the previous calculation, one can estimate the oxygen potential threshold of formation of $Cs_3Na(MoO_4)_2$ by reaction of sodium with Cs_2MoO_4 and MoO_2 at intermediate burnup, and with MoO_3 at very high
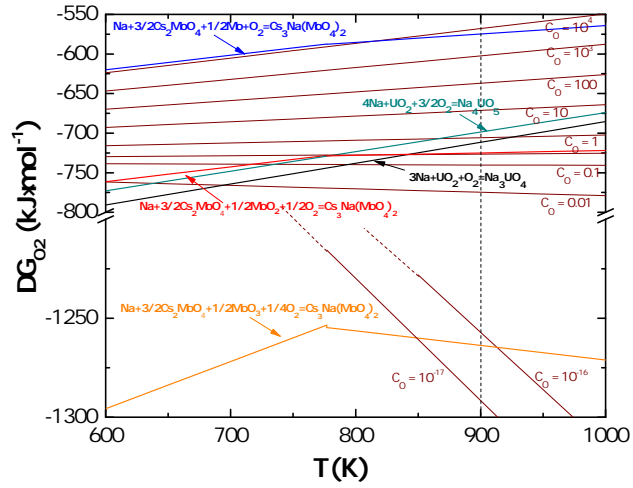
Figure 7: Calculated oxygen potential thresholds for the formation of $Cs_3Na(MoO_4)_2$ and sodium uranate Na_3UO_4 and Na_4UO_5 [30], and comparison with the oxygen levels in liquid sodium (C_0 from 0.01 to 1000 wppm), considering the solubility equation of Noden [27, 28]. Note that the slight mismatch at $T = 777$ K between the oxygen potential threshold equations for the formation of $Cs_3Na(MoO_4)_2(cr)$ and $Cs_3Na(MoO_4)_2(l)$ from MoO_3, Cs_2MoO_4 and Na(l) comes from the slight mismatch between the fitted equations for the Gibbs energies of formation at the melting temperature.

burnup, which corresponds to the following equilibrium reactions:

$$Na(l, O \text{ in sln}) + 3/2Cs_2MoO_4(cr) + 1/2MoO_2(cr) + 1/2O_2(\text{dissolved in Na}) \rightleftharpoons Cs_3Na(MoO_4)_2(l)$$
$$(5)$$

$$Na(l, O \text{ in sln}) + 3/2Cs_2MoO_4(cr) + 1/2MoO_3(cr) + 1/4O_2(\text{dissolved in Na}) \rightleftharpoons Cs_3Na(MoO_4)_2(l)$$
$$(6)$$
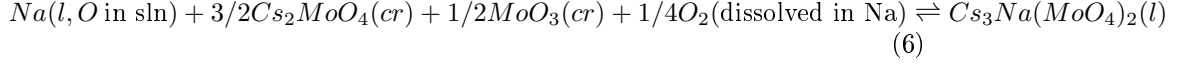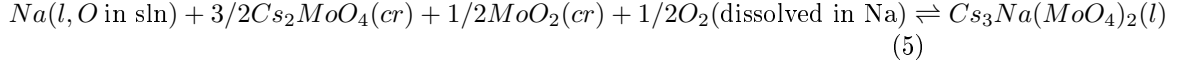
The equilibrium oxygen potentials for these reactions are respectively:

$$\Delta\overline{G_{O_2}^{eq}}(T) = 2\Delta_f G_m^o(Cs_3Na(MoO_4)_2, l, T) - 3\Delta_f G_m^o(Cs_2MoO_4, cr, T) - \Delta_f G_m^o(MoO_2, cr, T)$$
$$(7)$$

$$\Delta\overline{G_{O_2}^{eq}}(T) = 4\Delta_f G_m^o(Cs_3Na(MoO_4)_2, l, T) - 6\Delta_f G_m^o(Cs_2MoO_4, cr, T) - 2\Delta_f G_m^o(MoO_3, cr, T)$$
$$(8)$$

Using the thermodynamic functions listed in Table C.1 and C.2, the corresponding oxygen potential thresholds of formation of $Cs_3Na(MoO_4)_2$ from reaction with MoO_2 were derived as $\Delta\overline{G_{O_2}^{eq}}(T/K) = -873666 + 187.21\,T$ J·mol^{-1} in the temperature range T=(371-777) K, and $\Delta\overline{G_{O_2}^{eq}}(T/K) = -752841 + 30.93\,T$ J·mol^{-1} for T>777 K. The reaction with MoO_3 yields $\Delta\overline{G_{O_2}^{eq}}(T/K) = -1439081 + 238.88\,T$ J·mol^{-1} in the temperature range T=(371-777) K, and $\Delta\overline{G_{O_2}^{eq}}(T/K) = -1197432 - 73.68\,T$ J·mol^{-1} for T>777 K. When comparing with the oxygen levels in liquid sodium (Figure 7), one can see that an oxygen concentration of about 0.25 wppm is sufficient at T=900 K to form $Cs_3Na(MoO_4)_2$ from MoO_2, hence levels in the typical operating range of SFRs. It is interesting to point out that this oxygen threshold is found slightly below that of Na_3UO_4 and Na_4UO_5, two sodium uranate phases which can form in the fuel pin of SFRs by reaction between sodium coolant and hyperstoichiometric uranium dioxide, as shown by the recent studies of [30]. The oxygen level required to form $Cs_3Na(MoO_4)_2$ from MoO_3 (between 10^{-17} and 10^{-16} wppm at 900 K) is many orders of magnitude lower than the operating levels. This reaction is therefore unavoidable at high burnup.

4. Conclusions

A refinement of the crystal structure of the newly reported phase $Cs_3Na(MoO_4)_2$ has been performed in this work from neutron diffraction data for the first time. High temperature X-ray diffraction measurements have revealed a moderate thermal expansion for this compound. The thermal expansion coefficients along the a and c axes of this trigonal phase were derived as α_a= 31·10^{-6} K^{-1} and α_c= 24·10^{-6} K^{-1}, respectively, in the temperature range T=(298-723) K. The existence of a phase transition around $T = 663$ K as reported by [10] is not supported by the present XRD, DSC, and Raman spectroscopy data, however. Finally, the formation of $Cs_3Na(MoO_4)_2$ at low burnup by reaction between sodium, cesium molybdate, and molybdenum metal has been excluded according to our thermodynamic equilibrium calculations. The oxygen potential threshold required

for the formation of this phase from liquid sodium, Cs_2MoO_4 and molybdenum dioxide at high burnup was derived as $\Delta\overline{G}^{eq}_{O_2}(T/K) = -752841 + 30.93\,T$ J·mol^{-1} for temperatures above T=777 K. This corresponds to oxygen levels of 0.25 wppm at T=900 K, which are levels typically encountered in SFRs. The situation is even more critical for the reaction of liquid sodium, Cs_2MoO_4 and molybdenum trioxide: $\Delta\overline{G}^{eq}_{O_2}(T/K) = -1197432 - 73.68\,T$ J·mol^{-1}, which corresponds to oxygen levels between 10^{-17} and 10^{-16} wppm at 900 K. The thermodynamic driving force for the formation of this quaternary phase at high burnup following a breach of the cladding material is therefore high. The still poorly understood mechanism for the reaction of liquid sodium with the JOG phase should hence be re-investigated in the light of these new findings.

5. Acknowledgements

Appendices

A. Evolution of the lattice parameters of $Cs_3Na(MoO_4)_2$ as a function of temperature as derived from Rietveld refinement of the XRD data.

Table A.1: Summary of lattice parameters of $Cs_3Na(MoO_4)_2$ as a function of temperature.

T(K)	a (Å)	c (Å)
298	6.34252(4)	8.21761(6)
373	6.35676(4)	8.22996(6)
423	6.36498(5)	8.23748(7)
473	6.37421(4)	8.24623(6)
523	6.38403(4)	8.25584(6)
573	6.39504(3)	8.26705(5)
623	6.40438(3)	8.27679(4)
653	6.40897(5)	8.28176(7)
673	6.41486(5)	8.28791(8)
693	6.42047(6)	8.29368(9)
723	6.42759(6)	8.30100(9)

B. Variation of the vibration modes frequency of $Cs_3Na(MoO4)_2$ versus temperature: (a) bending and (b) stretching modes.
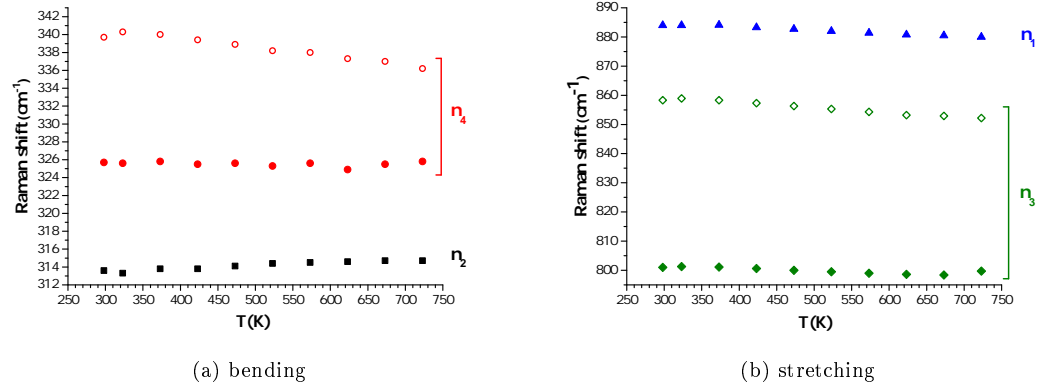

(a) bending

(b) stretching

Figure B.1: Variation of the vibration modes frequency of $Cs_3Na(MoO4)_2$ versus temperature: (a) bending and (b) stretching modes.

Table C.1: Summary of thermodynamic data for pure elements and oxides selected in the present work for the equilibrium calculations.

Phase	$\Delta_f H_m^o(298.15K)/$ $(kJ \cdot mol^{-1})$	$S_m^o(298.15K)/$ $(J \cdot K \cdot mol^{-1})$	$\Delta_{fus} H_m^o(T_{fus})/$ $(kJ \cdot mol^{-1})$	Ref.
β-Na(cr)	0	51.3 ± 0.2	-	[34–36]
Na(l)	-	-	2.598 ± 0.005 (370.9 K)	[37, 38]
Cs(cr)	0	85.23 ± 0.40	-	[35]
Cs(l)	-	-	2.096 (301.59 K)	[39]
Mo(cr)	0	28.56 ± 0.08	-	[38]
O_2(g)	0	205.152 ± 0.005	-	[35]
MoO_2(cr)	-589.5 ± 1.0	46.46 ± 0.42	-	[38]
MoO_3(cr)	-745.0 ± 1.0	77.76 ± 1.30	-	[38]
Cs_2MoO_4(cr)	-1514.7 ± 1.5	248.35 ± 0.30	31.8 ± 0.8 (1229.5 ± 0.2 K)	[18, 38]
Na_2MoO_4(cr)	-1466.5 ± 1.3	159.4 ± 1.2	21.7 ± 0.3^a (961 ± 1 K)^a	[18, 40], This work
$Cs_3Na(MoO_4)_2$(cr)	-2998.5 ± 3.0	467.2 ± 6.8	39.0 ± 1.0^b (777 ± 5 K)	[18], This work

The reported uncertainties correspond to standard uncertainties.

[a] Average value derived in this work based on the results of [41], [42], [43], [44].

[b] Value estimated in this work as described in Appendix D.

C. Thermodynamic functions used for the equilibrium calculations

Table C.2: Summary of heat capacity data for pure elements and oxides selected in the present work for the equilibrium calculations.

Phase	$C_{p,m}=A+B\cdot T+C\cdot T^{-2}+D\cdot T^2+E\cdot T^{-3}/J\cdot K\cdot mol^{-1}$					Temp. range/K	Ref.
	A	B	C	D	E		
β-Na(cr)	51.03936	$-14.46133\cdot10^{-2}$	-264307.5	$2.618297\cdot10^{-4}$		298.15-370.9	[36]
Na(l)	38.11988	$-19.49171\cdot10^{-3}$	-68684.96	$1.023984\cdot10^{-5}$		370.9-3000	[36]
Cs(cr)	90.52126	$-40.58844\cdot10^{-2}$	-490490.3	$7.67446\cdot10^{-4}$		298.15-301.59	[39]
Cs(l)	46.72733	$-40.86538\cdot10^{-3}$	-363055.7	$2.444908\cdot10^{-5}$		301.59-2000	[39]
Mo(cr)	23.56414	$6.8868\cdot10^{-3}$	-131625	$-3.39771\cdot10^{-6}$	$1.57112\cdot10^{-9}$	298.15-2896	[38]
O_2(g)	22.25862	$20.47734\cdot10^{-3}$	153499.1	$-8.039682\cdot10^{-6}$		298.15-900	[ref]
MoO_2(cr)	64.272	$18.03714\cdot10^{-3}$	-1207430			298.15-1803	[38]
MoO_3(cr)	77.731	$30.454\cdot10^{-3}$	-1060520			298.15-1074	[38]
Cs_2MoO_4(cr)	95.9182	$18.82224\cdot10^{-2}$	-95472	$-7.0314\cdot10^{-5}$		298.15-1229.5	[33]
Cs_2MoO_4(l)	210.154					>1229.5	[38]
Na_2MoO_4(cr)	143.947	$74.319\cdot10^{-3}$	-1873920	$-1.4088\cdot10^{-5}$		298.15-961	This work[a]
Na_2MoO_4(l)	213.384					>961	[45]
$Cs_3Na(MoO_4)_2$(cr)	292.0938	$12.334323\cdot10^{-2}$	-2661642	$-1.263059\cdot10^{-5}$		298.15-777	This work[b]
$Cs_3Na(MoO_4)_2$(l)	421.923					>777	This work[c]

[a] Function derived using the Neumann-Kopp rule applied to MoO_3 [38] and Na_2O [46].

[b] Function derived using the Neumann-Kopp rule applied to Cs_2MoO_4(cr) [33] and Na_2MoO_4(cr).

[c] Function derived using the Neumann-Kopp rule applied to Cs_2MoO_4(l) [38] and Na_2MoO_4(l) [45].

D. Estimated enthalpy of fusion for $Cs_3Na(MoO_4)_2$

The calculation of the margin to the safe operation of SFRs requires to estimate the thermodynamic functions of $Cs_3Na(MoO_4)_2$ in the liquid state, in particular the fusion enthalpy at the transition temperature $T_{fus} = (777 \pm 5)$ K.

To this end, the entropy of fusion of $Cs_3Na(MoO_4)_2$ was estimated with a linear combination of the fusion entropies of Cs_2MoO_4 and Na_2MoO_4:

$$\Delta_{fus}S_m^o(Cs_3Na(MoO_4)_2, T_{fus}) = \frac{3}{2}\Delta_{fus}S_m^o(Cs_2MoO_4, T_{fus}) + \frac{1}{2}\Delta_{fus}S_m^o(Na_2MoO_4, T_{fus})$$
(A.1)

The fusion entropy of Cs_2MoO_4 is $\Delta_{fus}S_m^o(Cs_2MoO_4, T_{fus}) = (25.9 \pm 0.7)$ $J\cdot K^{-1}\cdot mol^{-1}$ based on the selected data by Cordfunke and Konings [38]. The transition temperature and enthalpy of fusion of Na_2MoO_4 were measured by several authors using quantitative Differential Thermal Analysis (DTA) [41], drop calorimetry [42], high-temperature solid-liquid mixing microcalorimetry [43], and Differential Scanning Calorimetry [44]. Those data are summarized in Table C.3. The average value was selected in this work. Note that the latter value is very close to the one obtained by drop calorimetry [42], which is probably the most accurate. The corresponding entropy of fusion is $\Delta_{fus}S_m^o(Na_2MoO_4, T_{fus}) = (22.6 \pm 1.0)$ $J\cdot K^{-1}\cdot mol^{-1}$, a value very similar to that for Cs_2MoO_4. This leads to $\Delta_{fus}S_m^o(Cs_3Na(MoO_4)_2, T_{fus}) = (50.2 \pm 1.2)$ $J\cdot K^{-1}\cdot mol^{-1}$. Fi-

Table C.3: Summary of fusion temperatures and fusion enthalpies reported in the literature for Na_2MoO_4.

T_{tr}/K	$\Delta_{fus}H_m^o(T_{fus})/(kJ \cdot mol^{-1})$	Ref.
966 ± 2	24.43	[41]
962 ± 3	21.42 ± 0.5	[42]
959 ± 2	20.4 ± 0.4	[43]
957 ± 1	20.73 ± 1.14	[44]
$\mathbf{961 \pm 1}$	$\mathbf{21.7 \pm 0.3}$	This work

[a] Average value derived in this work based on the results of [41], [42], [43], [44].

nally, the enthalpy of fusion of $Cs_3Na(MoO_4)_2$ is derived as $\mathbf{\Delta_{fus}H_m^o(Cs_3Na(MoO_4)_2,}$ $\mathbf{T}_{fus}) = \mathbf{(39.0 \pm 1.0)\ kJ \cdot mol^{-1}}$.

6. References

[1] Z. Wang, H. Liang, M. Gong, and Q. Su. Journal of Alloys and Compounds 432(1-2) (2007) 308–312.

[2] C. Guo, H. K. Yang, and J.-H. Jeong. Journal of Luminescence 130(8) (2010) 1390–1393.

[3] Y. K. Voron´ko, K. A. Subbotin, V. E. Shukshin, D. A. Lis, S. N. Ushakov, A. V. Popov, and E. V. Zharikov. Optical Materials 29(2-3) (2006) 246–252.

[4] C. Cascales, A. M. Blas, M. Rico, V. Volkov, and C. Zaldo. Optical Materials 27(11) (2005) 1672–1680.

[5] V. A. Isupov. Ferroelectrics 321 (2005) 63–90.

[6] V. A. Isupov. Ferroelectrics 322 (2005) 83–114.

[7] E. F. Dudnik and G. A. Kiosse. Ferroelectrics 48 (1983) 33–48.

[8] Z. A. Solodovnikova, S. F. Solodovnikov, and E. S.Zolotova. Acta Crystallogr. C 62 (2006) 16–18.

[9] S. F. Solodovnikov, E. G. Khaikina, Z. A. Solodovnikova, Yu. M. Kadyrova, K. M. Khalbaeva, and E. S. Zolotova. Dokl. Chem. 416 (2007) 207–212.

[10] E. S. Zolotova, Z. A. Solodovnikova, V. N. Yudin, S. F. Solodovnikov, E. G. Khaikina, O. M. Basovich, I. V. Korolkov, and I. Y. Filatova. J. Solid State Chem. 233 (2016) 23–29.

[11] M. Tourasse, M. Boidron, and B. Pasquet. J. Nucl. Mater. 188 (1992) 49–57.

[12] Tam Ngoc Pham Thi. *Caractérisation et modélisation du comportement thermodynamique du combustible RNR-Na sous irradiation*. PhD thesis, Ecole Doctorale Physique et Sciences de la Matière (Aix-Marseille University), (2014).

[13] J.-C. Dumas. *Etude des conditions de formation du Joint-Oxyde-Gaine dans les combustibles oxydes mixtes des reacteurs à neutrons rapides, observations et proposition d'un modèle de comportement des produits de fission volatils.* PhD thesis, Institut national polytechnique de Grenoble, Grenoble, France, (1995).

[14] Y. Guerin. Comprehensive Nuclear Materials, Chapter 2.21: Fuel performance of Fast Spectrum Oxide Fuel, Elsevier, (2012).

[15] F. Tête. *La réaction Cs2MoO4/Na: Application à l'intéraction combustible/sodium lors d'une rupture de gaine à fort taux de combustible dans un RNR.* PhD thesis, Université d'Aix-Marseille 1, (1999).

[16] H. Kleykamp. J. Nucl. Mater. 248 (1997) 209–213.

[17] R. G. Samureva, R. M. Zharkova, and V. E. Plyushchev. Russian Journal of Inorganic Chemistry 1444 (1964) 9.

[18] A. L. Smith, M.-C. Pignié, L. van Eijck, J.-C. Griveau, E. Colineau, and R. J. M. Konings. J. Chem. Thermodyn. 120 (2018) 205–216.

[19] G. Wallez, P. E. Raison, A. L. Smith, N. Clavier, and N. Dacheux. J. Solid State Chem. 215 (2014) 225–230.

[20] L. van Eijck, L. D. Cussen, G. J. Sykora, E. M. Schooneveld, N. J. Rhodes, A. A. van Well, and C. Pappas. J. Appl. Crystallogr. 49 (2016) 1398–1401.

[21] J. Rodriguez-Carvajal. Physica B 192 (1993) 55–69.

[22] O. Beneš, R. J. M. Konings, S. Wurzer, M. Sierig, and A. Dockendorf. Thermochim. Acta 509(1-2) (2010) 62–66.

[23] M. Liégeois-Duyckaerts and P. Tarte. Spectrochim. Acta 28A (1972) 2037–2051.

[24] T. T. Basiev, A. A. Sobol ans Yu. K. Voronko, and P. G. Zverev. Opt. Mater. 15 (2000) 205–216.

[25] G. D. Saraiva, W. Paraguassa, M. Maczka, P. T. C. Freire, J. A. Lima (Jr.), C. W. A. Paschoal, J. Mendes Filho, and A. G. Souza Filho. J. Raman Spectrosc. 39 (2008) 937–941.

[26] G. D. Saraiva, W. Paraguassu, M. Maczka, P. T. C. Freir, F. F. de Sousa, and J. Mendes Filho. J. Raman Spectrosc. 42 (2011) 1114.

[27] J. D. Noden. J. Brit. Nucl. Energy Soc. 12(1) (1973) 57–62.

[28] J. D. Noden. J. Brit. Nucl. Energy Soc. 12(1) (1973) 329–331.

[29] M. G. Adamson, M. A. Mignanelli, P. E. Potter, and M. H. Rand. J. Nucl. Mater. 97 (1981) 203–212.

[30] A. L. Smith, C. Guéneau, J.-L. Flèche, S. Chatain, O. Beneš, and R. J. M. Konings. J. Chem. Thermodyn. (2017) doi.org/10.1016/j.jct.2017.04.003.

[31] H. Kleykamp. KfK 31 (1990) 4701.

[32] H. A. Wriedt. Bull. Alloy Phase Diagrams 8(3) (1987) 234–246.

[33] OECD, NEA, Thermodynamics of Advanced Fuels - International Database (TAF-ID), www.oecd-nea.org/science/taf-id/), Technical report.

[34] J. D. Cox, D. D. Wagman, and V. A. Medvedev. Hemisphere Publishing Corp, (1989).

[35] R. Guillaumont, T. Fanghänel, J. Fuger, I. Grenthe, V. Neck, D. A. Palmer, and M. H. Rand. OECD Nuclear Energy Agency, Data Bank, (2003).

[36] A. Dinsdale. Calphad 15 (1991) 317–425.

[37] O. Knacke, O. Kubaschewski, and K. Hesselman. Springer-Verlag, second edition, (1991).

[38] E. H. P. Cordfunke and R. J. M. Konings. North Holland, (1990).

[39] A. T. Dinsdale. Calphad 15(4) (1991) 317–425.

[40] W. W. Weller and E. G. King. U. S. Bureau of Mines, Technical Report RI-6245, (1963).

[41] R. Riccardi and C. Sinistri. Ric. Sci. Rend. Sez. A 8(5) (1965) 1026.

[42] L. Denielou, Y. Fournier, J.-P. Petitet, and Ch. Tequi. C. R. Acad. Sci. 272(23) (1971) 1855.

[43] S. Julsrud and O. J. Kleppa. Acta Chem. Scand. 35A(9) (1981) 669.

[44] A. V. Khoroshilov, G. A. Sharpataya, K. S. Gavrichev, and M. A. Ryumin. Russ. J. Inorg. Chem. 57(8) (2012) 1123–1127.

[45] I. Barin. VCH Verlagsgesellschaft mbH, Weinheim & VCH Publishers, Inc., New York, third edition, (1995).

[46] M. W. Chase. Nist-janaf thermochemical tables, american chemical society, american institute of physics, national bureau of standarts, 4th edition, (1998).